

Thermal conductivity of iron under the Earth's inner core pressure

Cui-E Hu(胡翠娥), Mu-Xin Jiao(焦亩鑫), Xue-Nan Yang(杨学楠), Zhao-Yi Zeng(曾召益), and Jun Chen(陈军)
Citation: Chin. Phys. B, 2024, 33 (**10**): 106501. DOI: 10.1088/1674-1056/ad6078
Journal homepage: http://cpb.iphy.ac.cn; http://iopscience.iop.org/cpb

What follows is a list of articles you may be interested in

Local thermal conductivity of inhomogeneous nano-fluidic films:A density functional theory perspective

Zongli Sun(孙宗利), Yanshuang Kang(康艳霜), and Yanmei Kang(康艳梅)
Chin. Phys. B, 2024, 33 (**4**): 046503. DOI: 10.1088/1674-1056/ad18a9

Wide frequency phonons manipulation in Si nanowire by introducing nanopillars and nanoparticles

Yatao Li(李亚涛), Yingguang Liu(刘英光), Xin Li(李鑫), Hengxuan Li(李亨宣), Zhixiang Wang(王志香), and Jiuyi Zhang(张久意)
Chin. Phys. B, 2024, 33 (**4**): 046502. DOI: 10.1088/1674-1056/ad0290

Phonon transport properties of Janus Pb_2XAs(X = P, Sb, and Bi) monolayers: A DFT study

Jiaxin Geng(耿嘉鑫), Pei Zhang(张培), Zhunyun Tang(汤准韵), and Tao Ouyang(欧阳滔)
Chin. Phys. B, 2024, 33 (**4**): 046501. DOI: 10.1088/1674-1056/ad2260

Molecular dynamics study on the dependence of thermal conductivity on size and strain in GaN nanofilms

Ying Tang(唐莹), Junkun Liu(刘俊坤), Zihao Yu(于子皓), Ligang Sun(孙李刚), and Linli Zhu(朱林利)
Chin. Phys. B, 2023, 32 (**6**): 066502. DOI: 10.1088/1674-1056/acbf26

Lattice thermal conductivity switching via structural phase transition in ferromagnetic VI_3

Chao Wu(吴超) and Chenhan Liu(刘晨晗)
Chin. Phys. B, 2023, 32 (**5**): 056502. DOI: 10.1088/1674-1056/acb764

Thermal conductivity of iron under the Earth's inner core pressure

Cui-E Hu(胡翠娥)[1], Mu-Xin Jiao(焦亩鑫)[1], Xue-Nan Yang(杨学楠)[1], Zhao-Yi Zeng(曾召益)[1,2,†], and Jun Chen(陈军)[2,3,‡]

[1] *College of Physics and Electronic Engineering, Chongqing Normal University, Chongqing* 400047, *China*
[2] *Laboratory of Computational Physics, Institute of Applied Physics and Computational Mathematics, Beijing* 100088, *China*
[3] *Center for Applied Physics and Technology, Peking University, Beijing* 100071, *China*

(Received 18 April 2024; revised manuscript received 20 June 2024; accepted manuscript online 9 July 2024)

The thermal conductivity of ε-iron at high pressure and high temperature is a key parameter to constrain the dynamics and thermal evolution of the Earth's core. In this work, we use first-principles calculations to study the Hugoniot sound velocity and the thermal transport properties of ε-iron. The total thermal conductivity considering lattice vibration is 200 W/mK at the Earth's inner core conditions. The suppressed anharmonic interactions can significantly enhance the lattice thermal conductivity under high pressure, and the contribution of the lattice thermal conductivity should not be ignored under the Earth's core conditions.

Keywords: thermal conductivity, first-principles, high pressure and high temperature

PACS: 65.40.–b, 62.20.–x, 62.50.–p, 63.20.dk **DOI:** 10.1088/1674-1056/ad6078

1. Introduction

Iron (Fe) is a material of key importance to condensed matter physics and Earth sciences, which is reported to be the major element in Earth's core. The solid inner core is almost fully filled with Fe, the other elements are commonly assumed to be 5% to 10% Ni and 2% to 4% light elements (e.g., Si, C, S).[1–3] To investigate the properties of Fe under the Earth's core conditions, it is essential to know the structure of Fe under high pressure. The stable phase of Fe in the inner core is widely reported to be ε-Fe with a hexagonal-closed-packed (hcp) structure.[4–9] However, this conclusion has been challenged by some theoretical investigations. Vocadlo *et al.*[10] and Belonoshko *et al.*[11,12] proposed that body-centered cubic (bcc) Fe may be stable under inner core conditions. Previously, we calculated the phonon dispersion of bcc-Fe and hcp-Fe under high temperature and high pressure with the self-consistent *ab initio* lattice dynamics method.[13] Though the bcc-Fe and hcp-Fe are both dynamically stable under the Earth's core conditions, the free energy of hcp-Fe is lower than that of bcc-Fe. We also investigated the equation of state, elastic constants, phase transition and magnetic of Fe under high pressure,[13–15] and all the results showed that the most stable phase is nonmagnetic ε-Fe at high pressure.[15] Therefore, we restrict the structure to ε-Fe in this work.

The thermal conductivity of Fe under high pressure and high temperature is of central importance to understanding the thermal evolution of the Earth's core and the energetics of the geomagnetic field. In the past few years, many investigations of Fe under the Earth's inner core conditions have been done from theory and experiment, but there is still a significant discrepancy in thermal conductivity at the core–mantle boundary (CMB).[16–23] By the laser heated diamond anvil cell (DAC) experiments, the data of thermal conductivity are 33 ± 7 W/(m·K)[22] at the CMB conditions and 70–80 W/(m·K)[24] (with an uncertainty of 40%) up to 134 GPa. In contrast, through the resistivity measurements in DAC, thermal conductivity was reported up to 226^{+71}_{-31} W/(m·K).[20] But with similar experiments, Zhang *et al.* found that the thermal conductivity of Fe was $\sim 100 \pm 10$ W/(m·K).[19] Theoretically, the thermal conductivity near the CMB estimated from first principles was 150 W/(m·K),[21,23] $\sim 100 \pm 10$ W/(m·K),[19] and 97 ± 10 W/(m·K),[18] respectively. However, these data are three to five times higher than geophysical estimates and shock experiments. For metal, the thermal conductivity is mainly attributed to the electronic conductivity, and the contribution of the lattice thermal conductivity is ignored. Because of the harmonic phonon interactions, the heat transfer processes have no thermal resistance, which means the infinite thermal conductivity. The suppressed anharmonic interactions can enhance the lattice thermal conductivity obviously under high pressure. In this work, we calculated the thermal conductivity of Fe under the Earth's core condition with the Boltzmann transport theory.

2. Theoretical methods

All the calculations are performed by the Vienna *ab initio* simulation package (VASP). The exchange–correlation interactions are treated using the spin-polarized generalized gra-

†Corresponding author. E-mail: zhaoyizeng@cqnu.edu.cn
‡Corresponding author. E-mail: jun_chen@iapcm.ac.cn

© 2024 Chinese Physical Society and IOP Publishing Ltd

dient approximation within the Perdew–Burke–Ernzerhof formulation and the project augmented wave. The plane-wave cutoff energy is set to 500 eV and the k-point sampling grid in the Brillouin zone is chosen to be $11\times11\times11$ in the geometry optimization. The energy convergence criterion is set to a precision of 10^{-6} eV and the forces on all relaxed atoms are less than 0.001 eV/Å. Based on a full iterative solution to the Boltzmann transport equation, the phonon dispersions of ε-Fe are obtained by finite displacement method with a $4\times4\times4$ supercell containing 128 independent atoms. The third-order force constants are also considered with 128 atoms. The k-point meshes of $9\times9\times9$ are selected for both second-order force and third-order force calculations.

The Helmholtz free energy F can be accurately separated as

$$F(V,T) = E_{\text{static}}(V) + F_{\text{phon}}(V,T) + F_{\text{elec}}(V,T), \tag{1}$$

where $E_{\text{static}}(V)$ is the energy of a static lattice at zero temperature T and volume V, $F_{\text{elec}}(V,T)$ is the thermal free energy arising from electronic excitations. Both $E_{\text{static}}(V)$ and $F_{\text{elec}}(V,T)$ can be obtained from static first-principles calculations directly. The nonequilibrium vibrational contribution $F_{\text{phon}}(V,T)$ is given by

$$F_{\text{phon}}(V,T) = \frac{k_{\text{B}}T}{\Omega}\int_{\text{BZ}} \mathrm{d}q \sum_s \ln(2\sinh(\hbar\omega_{qs}/(2k_{\text{B}}T))), \tag{2}$$

where Ω is the volume of the Brillouin Zone, k_{B} is the Boltzmann constant, $\hbar$ is the Plank constant and ω_{qs} are the phonon frequencies. This is obtained within the quasiharmonic approximation (QHA) by small displacements method.

The elastic constants are defined by means of a Taylor expansion of the total energy, $E(V,\delta)$, for the system with respect to a small strain δ of the lattice primitive cell volume V. The energy of a strained system is expressed as

$$E(V,\delta) = E(V_0,0) + V_0\left[\sum_i \tau_i\xi_i\delta_i + \frac{1}{2}\sum_{ij} C_{ij}\delta_i\xi_j\delta_j\right], \tag{3}$$

where $E(V_0,0)$ is the energy of the unstrained system with equilibrium volume V_0, τ_i is an element in the stress tensor, and ξ_i is a factor to take care of Voigt index. The elastic strains are generated by the VASPKIT code.[25]

The lattice thermal conductivity k_{l} can be obtained busing the phonon Boltzmann transport equation (BTE) given by[26]

$$k_{\text{l}} = \frac{1}{3N\Omega}\sum_q C_q \upsilon_q^2 \tau_q, \tag{4}$$

where Ω is the volume of the unit cell, N is the number of atoms, C_q is the heat capacity, υ_q is the group velocity and τ_q is the phonon relaxation time. The C_q can be evaluated from the phonon density of states. The υ_q are obtained by calculating the gradient of the phonon dispersion relation. The τ_q are calculated from Fermi's golden rule using the harmonic and third-order anharmonic force constants from DFT calculations. In this work, the phonon–phonon scattering contribution is considered, and the phonon–electron scattering process is neglected. The electrical thermal conductivity k_{e} and the electrical resistivity ρ are connected by the Wiedemann–Franz law

$$k_{\text{e}} = \frac{\pi^2}{3}\left(\frac{k_{\text{B}}}{3}\right)^2 \frac{T}{\rho}, \tag{5}$$

where T is the temperature. The electrical resistivity ρ is mainly attributed to the electron–electron scattering contribution. The electrical resistivity ρ can be obtained from the electrical conductivity tensor σ_{e} directly ($\rho = 1/\sigma_{\text{e}}$). The $\sigma_{\text{e}}/\tau_{\text{e}}$ can be obtained using the BTE with the relaxation time approximation, where τ_{e} is the electronic relaxation time. With this approximation, $(\sigma_{\text{e}}/\tau_{\text{e}})$ only depends on the electronic band structure and the values can be obtained from DFT-BTE calculations using VASP and the BoltzTrap code.[27]

3. Results and discussion

3.1. Hugoniot and sound velocity

The Earth's core is at extreme conditions of high temperatures and pressures. Under the Earth's core conditions, the variation of the axial ratio c/a is a direct response to the changes of elastic anisotropy. In present work, for a fixed axial ratio c/a, we calculate the total energies E at different cell volumes V, and then obtain the lowest energy for the given ratio c/a. The value of c/a is 1.603 at 135 GPa, and it increases a little with the increasing pressure up to Earth's inner core condition. The nearly constant value of the c/a ratio agrees with other data (1.596–1.608).[28–31] We calculated the phonon dispersions of ε-Fe at different pressures (Fig. 1). As the phase transition of Fe from bcc phase to hcp phase occurs at 13 GPa,[32] the obtained phonon dispersions in the present work started from this pressure. The frequency of phonon dispersion increases with the increasing pressure. Near the Γ point, the slope of the acoustic branch increases significantly, which shows that the group velocity increases with the increasing pressure.

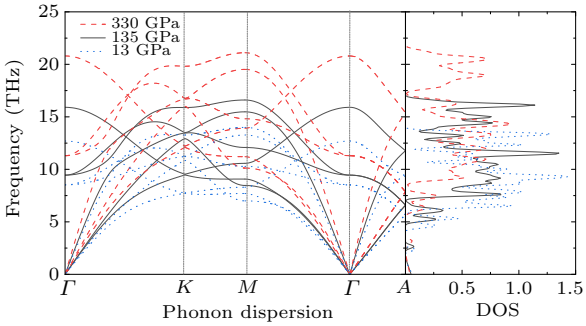


Fig. 1. The phonon dispersions and DOS of Fe.

In a shock wave experiment, conservation of mass, momentum, and energy require that the pressure P_H, the molar internal energy U_H, and the molar volume V_H in the compression wave are related by the Rankine–Hugoniot formula

$$U_H - U_0 = \frac{1}{2}(P_H + P_0)(V_0 - V_H), \tag{6}$$

where U_0 and V_0 are the molar internal energy and volume in the initial state (zero pressure P_0) before the arrival of the wave. Considering the thermal free energy arising from electronic excitations and phonon contributions, the obtained Hugoniot curves of Fe are shown in Fig. 2. At 135 GPa, the present Hugoniot temperature (T_H) is about 2500 K, which is consistent with the data from the experimental,[33] theoretical results[34] and the preliminary reference Earth model (PREM)[35] at the CMB. At 330 GPa, the present T_H is close to 6500 K, which agrees with the temperature ($\sim$ 6000 K) at ICB.[36]

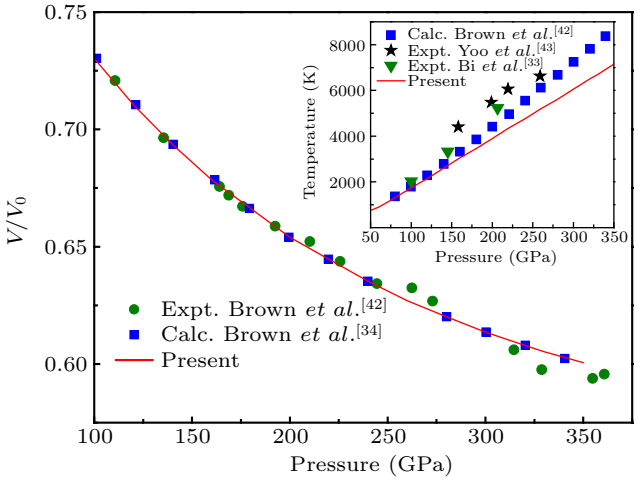


Fig. 2. The Hugoniot of Fe. The green circles are experimental data by Brown *et al.*,[42] the blue squares are theoretical values,[34] the green triangle and black stars are experimental data.[33,43]

We calculate the elastic constants along Hugoniot, and then obtain the bulk and shear modulus (B and G) from the elastic constants. The compressional sound velocity V_P and shear sound velocity V_S can be obtained as follows:

$$V_P = \left[(B + 4G/3)/\rho\right]^{1/2}, \tag{7}$$

$$V_S = (G/\rho)^{1/2}, \tag{8}$$

where ρ is the density. The sound velocities along Hugoniot state are shown in Fig. 3. It can be seen that the sound velocities increase with the increasing pressure. Our results are generally consistent with the shock wave experimental data below 160 GPa.[3,7,8,34] The small discrepancies between our results and experimental data may be due to the fact that we neglected the electronic thermal effects when evaluating its elastic properties. Above 160 GPa, our results deviate from the experimental data. As those P–T conditions approach the region of shock-induced melting of Fe, the shock experimental data show nonlinear relation with pressure. Above 200 GPa, the shock shear sound velocities V_S decrease dramatically to zero, which indicates the melting of Fe.[3,7,8,34] In our model, the QHA for one phase cannot simulate the shock melting. However, our results can provide useful references for understanding the sound velocity under the Earth's core conditions. Under the ICB pressure, the V_P and V_S are about 12.2 km/s and 5.5 km/s, which generally agree with the data (6600 K at 360 GPa and 7000 K at 360 GPa) from *ab initio* molecular dynamics simulations (AIMD).[37] But our results are larger than that of PREM data.[35] The difference between our results and the PREM seismic data is marginally within mutual uncertainties. The differences may be accounted for by the presence of other light elements (e.g., S, Si and C) and heavy element alloy (e.g., Ni). Meanwhile, a possible explanation for the large discrepancy may be that parts of the inner core are partially molten. In order to understand the seismic data, further systematic studies are needed to improve our knowledge.

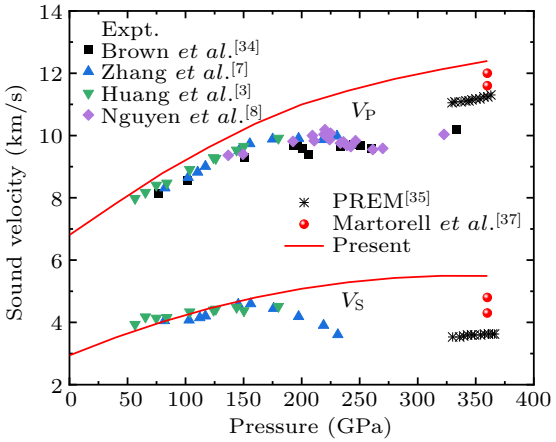


Fig. 3. The aggregate velocities versus pressure, compared with the shock experimental data[3,7,8,34] and the theoretical results (at 6600 K and 7000 K) from AIMD.[37] Preliminary reference Earth model (PREM) seismic data[35] are reported for comparison as crosses. The red line is the fitting curve from present data.

3.2. Thermal conductivity

The thermal conductivity of ε-Fe is crucial to understanding the thermal history of the core and the geodynamo. As shown in Fig. 4, the k_l increases linearly along Hugoniot curve. The increasing of the phonon group velocity surpasses the decreasing phonon scattering, and it becomes the main contribution for the increase of k_l. The data of the k_l are 6.05 W/(m·K) at CMB and 12.63 W/(m·K) at ICB, respectively. We analyzed the contribution of each phonon model (one longitudinal acoustic branch LA, and two transverse acoustic branches TA1, TA2) to the total lattice thermal conductivity, which is shown in Fig. 5(a). It is found that the acoustic branches dominate the contribution of the lattice thermal conductivity. The contribution of the acoustic branch to the lattice thermal conductivity is 81% at 135 GPa, and 92% at 330 GPa. The energy

of the optical branches is lower than that of acoustic branches, and thus it can be excited more easily. As shown in Fig. 5(b), the cumulative thermal conductivity is primarily governed by the acoustic phonon modes at low-frequency regions.

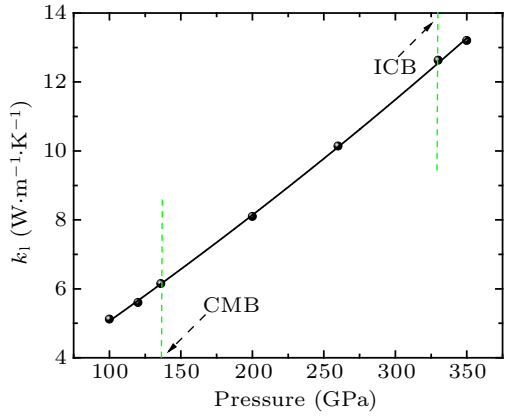


Fig. 4. The lattice thermal conductivity of Fe as a function of pressure.

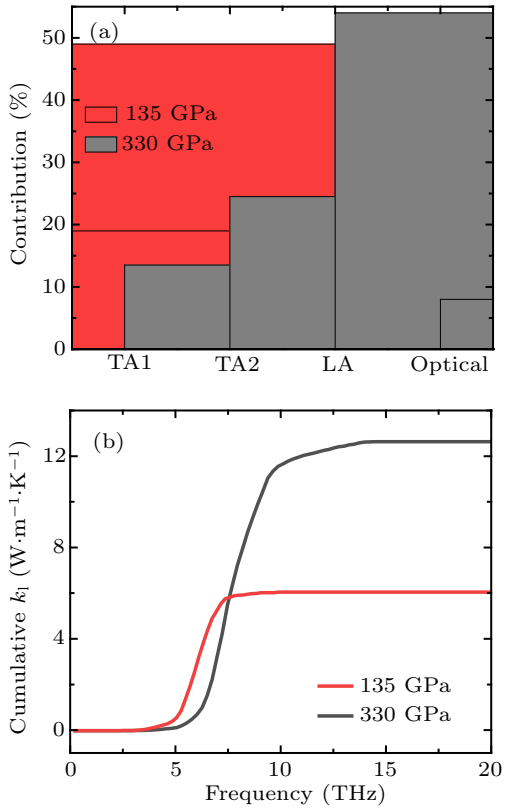


Fig. 5. (a) Contribution of phonon modes to the lattice thermal conductivity of ε-Fe, (b) the cumulative thermal conductivity of ε-Fe as a function of frequency.

To explore the physical mechanism of the thermal conductivity, we investigate the phonon group velocity, phonon scattering rate and Grüneisen parameter under high pressures. The group velocities v_g can be obtained from the slope of the phonon dispersion. The relationships between the phonon group velocities and frequencies are shown in Figs. 6(a) and 6(b). The group velocities of acoustic branches are larger than that of optical branches, which confirms that the acoustic branches play a major role in the lattice thermal conductivity. The group velocities of the LA branch are the highest of all phonon modes and the largest contribution to the lattice thermal conductivity is from the LA branch. Near the Γ point, the maximum of the group velocities at 135 GPa and 330 GPa are 5.72 km/s and 6.85 km/s, respectively.

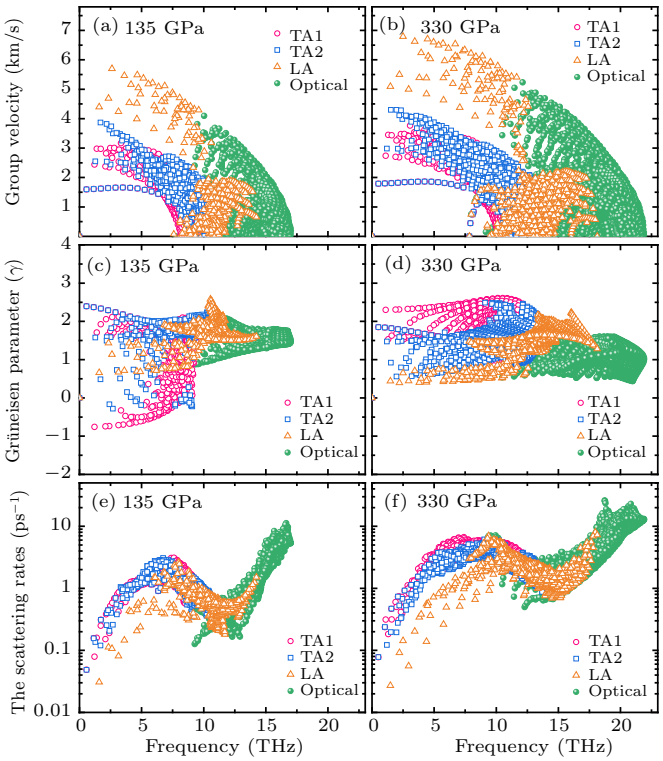


Fig. 6. The variations of group velocity (a) and (b), Grüneisen parameter (c) and (d), and phonon scattering rate (e) and (f) at 135 GPa and 330 GPa, respectively. The slid spheres are the data from optical branch. The open circles, open squares and open triangles are the data from longitudinal acoustic branch LA, two transverse acoustic branches TA1 and TA2, respectively.

The phonon scattering intensity is dependent on the mode-dependent Grüneisen parameter γ, which reflects the anharmonicity of the phonon. The γ can be obtained from the relationship between phonon frequency and volume change as follows:

$$\gamma = -\frac{\mathrm{d}\ln\omega}{\mathrm{d}\ln V}, \tag{9}$$

where ω is the frequency and V is volume. The relationships between Grüneisen parameter and frequencies are shown in Figs. 6(c) and 6(d). The negative value of the Grüneisen parameter at 135 GPa, which indicates the large anharmonic terms beyond third-order terms. However, the absence of negative Grüneisen parameters at 330 GPa indicates that the high pressure suppresses the anharmonicity.

The scattering rates at different pressures are shown in Figs. 6(e) and 6(f). It can be seen that the acoustic branch occupies the middle- and low-frequency portions and the optical branch occupies the high-frequency portion. As the fre-

quency increases, the scattering rates of acoustic branches increase gradually and remain between 1 ps^{-1} and 10 ps^{-1}. The phonon scattering increases under pressure, which is attributed to the increased anisotropy. As shown in our previous investigations, Fe is elastically anisotropic at the inner core.[14] At 135 GPa, the small phonon scattering rate results from the relatively isotropic phonon branches. Such phonon dispersions provide few scattering channels, so the scattering rate is small. However, at 330 GPa the three phonon branches are relatively far from each other. This change opens more scattering channels and the phonon–phonon scattering is consequently increased.

The electron thermal conductivity (k_e) is dominant in the thermal transport properties of ε-Fe. We obtained the electronic thermal conductivity k_e of ε-Fe along Hugoniot. At 135 GPa and 330 GPa, the data of electron thermal conductivity are 106 W/(m·K) and 108 W/(m·K), respectively. The results of the total thermal conductivity ($k = k_e + k_l$) are shown in Fig. 7. At the CMB conditions, the value of k is 112 W/(m·K), which is in agreement with the value of 97 ± 10 W/(m·K)[18] and 100 ± 10 W/(m·K).[19] Near the ICB, the value of k is 200 W/(m·K), which is consistent with the previous results.[23,38] The proportion of lattice thermal conductivity enhances from 5.4% at CMB up to 6.3% at ICB, which indicates that the contribution of the lattice thermal conductivity should not be ignored under Earth's core conditions. Our thermal conductivity at the CMB is 112 W/(m·K), and it can also verify the viewpoint that the geodynamo is driven by thermal convection.

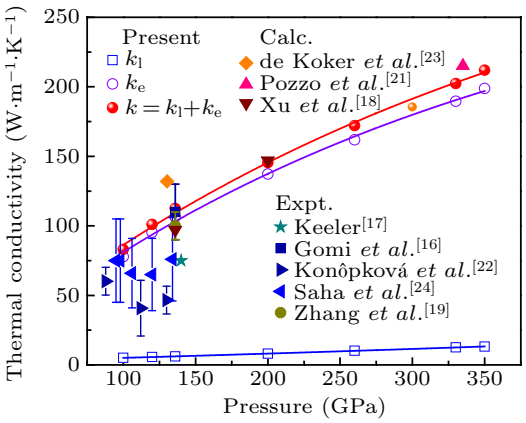


Fig. 7. Thermal conductivity of ε-Fe as a function of pressure. The stars,[17] squares,[16] right triangles,[22] left triangles,[24] and circles[19] are the experimental data. The diamonds,[23] up triangles,[21] and down triangles[18] are the theoretical data.

From thermal conductivity, the adiabatic heat flow (Q_a) of ε-Fe corresponding to the top of the liquid core can be obtained as follows:

$$Q_a(r) = 4\pi r^2 k \frac{g\gamma T}{\varphi}, \tag{10}$$

where r is the radius, γ is Grüneisen parameter, g is the gravitational acceleration ($g_{CMB} = 10.6823$ m/s^2) and ϕ is the seismic parameter ($\phi_{CMB} = 65.05$ km^2/s^2).[39] The high thermal conductivity 112 W/(m·K) at the CMB indicates an adiabatic heat flow Q_a of ~ 14.7 TW. While the present-day CMB heat flow across the lowermost mantle (Q_{CMB}) is constrained to be 10–12 TW based on the estimated thermal conductivity (~ 10 W/(m·K)) of the mantle minerals.[40] The geodynamo is maintained by fluid convection in the outer core. It is believed that the fluid convection is mainly driven by thermal or compositional buoyancy, where the former requires a higher Q_{CMB} than the Q_a based on the Schwarzschild criterion.[41] The high thermal conductivity of ε-Fe makes $Q_a > Q_{CMB}$, and thus hinders thermal convection. However, chemical buoyancy released at the ICB by inner core growth could still drive convection at depth. As a result, the present-day geodynamo would be mainly driven by compositional convection.

4. Conclusions

In summary, the phonon dispersion, Hugoniot equation of state and thermal transport properties of the ε-Fe were investigated by first-principles calculations together with Boltzmann transport theory. The phonon dispersion curves under high pressure show that the ε-Fe is a stable phase at Earth's core conditions. The Hugoniot sound velocities agree with the previous investigations. Considering the contribution of lattice vibration, the total thermal conductivity is much closer to the experimental data than the result which is obtained only by considering the electron thermal conductivity. The total thermal conductivity for ε-iron is 200 W/(m·K) at the ICB. The variation trend of lattice thermal conductivity is obviously affected by pressure. The suppressed anharmonic interactions can significantly enhance the lattice thermal conductivity under high pressure, and the contribution of the lattice thermal conductivity should not be ignored under the conditions of the Earth's core.

Acknowledgements

Project supported by the National Natural Science Foundation of China (Grant No. 12072044) and the Natural Science Foundation of Chongqing City (Grant No. cstc2020jcyj-msxmX0616).

References

[1] Hirose K, Labrosse S and Hernlund J 2013 *Annual Review of Earth and Planetary Sciences* **41** 657
[2] Poirier J P 1994 *Physics of the Earth and Planetary Interiors* **85** 319
[3] Huang H, Fan L, Liu X, Xu F, Wu Y, Yang G, Leng C, Wang Q, Weng J and Wang X 2022 *Nat. Commun.* **13** 616
[4] Mao H K, Shu J, Shen G, Hemley R J, Li B and Singh A K 1998 *Nature* **396** 741
[5] Alfè D, Price G D and Gillan M J 2001 *Phys. Rev. B* **64** 045123
[6] Zhang Y, Luo K, Hou M, Driscoll P, Salke N P, Minár J, Prakapenka V B, Greenberg E, Hemley R J and Cohen R E 2022 *Proc. Natl. Acad. Sci. USA* **119** e2119001119

[7] Zhang Y, Wang Y, Huang Y, Wang J, Liang Z, Hao L, Gao Z, Li J, Wu Q and Zhang H 2023 *Proc. Natl. Acad. Sci. USA* **120** e2309952120
[8] Nguyen J H and Holmes N C 2004 *Nature* **427** 339
[9] Tateno S, Hirose K, Ohishi Y and Tatsumi Y 2010 *Science* **330** 359
[10] Vočadlo L, Alfè D, Gillan M, Wood I, Brodholt J and Price G D 2003 *Nature* **424** 536
[11] Belonoshko A B, Ahuja R and Johansson B 2003 *Nature* **424** 1032
[12] Belonoshko A B, Lukinov T, Fu J, Zhao J, Davis S and Simak S I 2017 *Nature Geoscience* **10** 312
[13] Niu Z W, Zeng Z Y, Cai L C and Chen X R 2015 *Physics of the Earth and Planetary Interiors* **248** 12
[14] Chen X R, Zeng Z Y, Liu Z L, Cai L C and Jing F Q 2011 *Phys. Rev. B* **83** 132102
[15] Zeng Z Y, Hu C E, Chen X R, Cai L C and Jing F Q 2008 *J. Phys.: Condens. Matter* **20** 425217
[16] Gomi H, Ohta K, Hirose K, Labrosse S, Caracas R, Verstraete M J and Hernlund J W 2013 *Physics of the Earth and Planetary Interiors* **224** 0031
[17] Keeler R N 1971 *Physics of High Energy Density* **106**
[18] Xu J, Zhang P, Haule K, Minar J, Wimmer S, Ebert H and Cohen R E 2018 *Phys. Rev. Lett.* **121** 096601
[19] Zhang Y, Hou M, Liu G, Zhang C, Prakapenka V B, Greenberg E, Fei Y, Cohen R E and Lin J F 2020 *Phys. Rev. Lett.* **125** 078501
[20] Ohta K, Kuwayama Y, Hirose K, Shimizu K and Ohishi Y 2016 *Nature* **534** 95
[21] Pozzo M, Davies C J and Alfè D 2022 *Earth and Planetary Science Letters* **584** 117466
[22] Konôpková Z, McWilliams R S, Gómez-Pérez N and Goncharov A F 2016 *Nature* **534** 99
[23] De Koker N, Steinle-Neumann G and Vlček V 2012 *Proc. Natl. Acad. Sci. USA* **109** 4070
[24] Saha P, Mazumder A and Mukherjee G D 2020 *Geoscience Frontiers* **11** 1755
[25] Wang V, Xu N, Liu J C, Tang G and Geng W T 2021 *Computer Physics Communications* **267** 108033
[26] Li W, Carrete J, Katcho N A and Mingo N 2014 *Computer Physics Communications* **185** 1747
[27] Madsen G K and Singh D J 2006 *Computer Physics Communications* **175** 67
[28] Ma Y, Somayazulu M, Shen G, Mao H K, Shu J and Hemley R J 2004 *Physics of the Earth and Planetary Interiors* **143–144** 455
[29] Mao H K, Wu Y, Chen L C, Shu J F and Jephcoat A P 1990 *Journal of Geophysical Research: Solid Earth* **95** 21737
[30] Glazyrin K, Pourovskii L V, Dubrovinsky L, Narygina O, McCammon C, Hewener B, Schünemann V, Wolny J, Muffler K, Chumakov A I 2013 *Phys. Rev. Lett.* **110** 117206
[31] Yamazaki D, Ito E, Yoshino T, Yoneda A, Guo X, Zhang B, Sun W, Shimojuku A, Tsujino N and Kunimoto T 2012 *Geophysical Research Letters* **39** L20308
[32] Boettger J C and Wallace D C 1997 *Phys. Rev. B* **55** 2840
[33] Bi Y, Tan H and Jing F 2002 *J. Phys.: Condens. Matter* **14** 10849
[34] Brown J M and McQueen R G 1986 *Journal of Geophysical Research: Solid Earth* **91** 7485
[35] Dziewonski A M and Anderson D L 1981 *Physics of the Earth and Planetary Interiors* **25** 297
[36] Price G D, Alfè D, Vočadlo L and Gillan M 2004 *The Earth's Core: An Approach from First Principles*
[37] Martorell B, Vočadlo L, Brodholt J and Wood I G 2013 *Science* **342** 466
[38] Pozzo M, Davies C, Gubbins D and Alfè D 2012 *Nature* **485** 355
[39] Gomi H and Hirose K 2015 *Physics of the Earth and Planetary Interiors* **247** 2
[40] Hsieh W P, Deschamps F, Okuchi T and Lin J F 2018 *Proc. Natl. Acad. Sci. USA* **115** 4099
[41] Schatten K and Sofia S 1981 *Astrophysical Letters* **21** 93
[42] Brown J M, Fritz J N and Hixson R S 2000 *J. Appl. Phys.* **88** 5496
[43] Yoo C S, Holmes N C, Ross M, Webb D J and Pike C 1993 *Phys. Rev. Lett.* **70** 3931